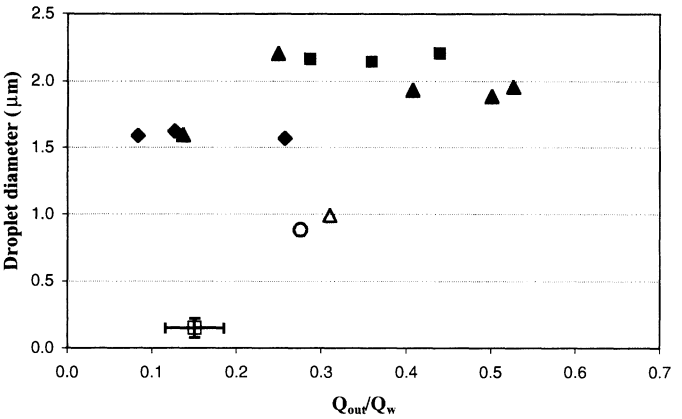

Fig. 6. Typical sizes of capsules of water surrounded by a thin shell of olive oil. ■, Q_w = 39.8e-12 $m^3 s^{-1}$; ▲, Q_w = 26.0e-12 $m^3 s^{-1}$; ◆, Q_w = 18.4e-12 $m^3 s^{-1}$; ○, Q_w = 17.8e-12 $m^3 s^{-1}$; △, Q_w = 25.5e-12 $m^3 s^{-1}$; and □, Q_w = 1.5e-12 $m^3 s^{-1}$.

fluid) with different electrical conductivities (0.14, 0.05, and 0.01 S m^{-1}). The horizontal axis represents the ratio Q_{out}/Q_w, where Q_w is the water flow rate and Q_{out} is the oil flow rate. The diameter is calculated from the measured current, flow rates, and electrical mobility. Filled symbols represent situations in which the flow rate of water is kept constant while the flow rate of olive oil is varied. Open symbols represent situations where both flow rates have been varied. The smallest capsule diameter attained during these exploratory experiments is about 0.150 μm, corresponding to a sphere of water of about 100 nm in diameter covered by a layer of oil whose thickness is about 25 nm. The dispersion of sizes, for each experiment, remains below 7%, except in the case of the smallest capsules (0.150 μm), because of limitations to properly controlling the flow rate of oil in this extreme case.

We have presented a technique to generate coaxial electrified liquid jets in the micrometer and submicrometer ranges by EHD. This method allows for a precise tailoring of both the outer and the outer-to-inner radius ratio by controlling the flow rates of both liquids and the applied voltage. A direct application to the production of monodisperse capsules in the micrometer range has been included. Although in this particular example, the outer fluid consists of a photopolymer, which is solidified under ultraviolet light, the use of different polymerization schemes is also applicable with this technique. Also, monodisperse compound droplets of water coated by olive oil, with sizes well in the submicrometer range, have been obtained. Both the amount of water and thickness of the coating oil layer can be well controlled.

References and Notes

1. H. Yosii *et al.*, *Inn. Food Sci. Em. Technol.* **2**, 55 (2001).
2. N. Hardas, S. Danviriyakul, J. L. Foley, W. W. Nawar, P. Chinachoti, *Lebensm.-Wiss. U.-Technol.* **33**, 506 (2000).
3. S. J. Lee, M. Rosemberg, *Lebensm.-Wiss. U.-Technol.* **33**, 80 (2000).
4. G. H. Wolters, W. M. Fritschy, D. Gerrits, R. Van Schilfgaarde, *J. Appl. Biomatter* **3**, 281 (1992).
5. E. Mathiowitz, *Encyclopedia of Controlled Drug Delivery* (Wiley, New York, 1999).
6. E. Mathiowitz *et al.*, *Nature* **386**, 410 (1997).
7. T. Jung *et al.*, *Eur. J. Pharm. Biopharm.* **50**, 147 (2000).
8. R. T. Bartus, M. A. Tracy, D. F. Emerich, S. E. Zale, *Science* **281**, 1161 (1998).
9. R. Langer, *Nature* **392**, 5 (1998).
10. T. Ciach, J. Wang, J. Marijnissen, *J. Aerosol Sci.* **32**, S1001 (2001).
11. Y. H. Lee, C. A. Kim, W. H. Jang, H. J. Choi, M. S. Jhon, *Polymer* **42**, 8277 (2001).
12. G. Burlak, S. Koshevaya, J. Sánchez-Mondragón, V. Grimalsky, *Opt. Commun.* **187**, 91 (2001).
13. R. A. Jain, *Biomaterials* **21**, 2475 (2000).
14. R. Gref *et al.*, *Science* **263**, 1600 (1994).
15. M. Aboubakar, F. Puisieux, P. Couvreur, C. Vauthier, *Int. J. Pharm.* **183**, 63 (1999).
16. G. E. Hildebrand, J. W. Tack, *Int. J. Pharm.* **196**, 173 (2000).
17. H. Reithmeier, J. Herrmann, A. Göpferich, *Int. J. Pharm.* **218**, 133 (2001).
18. M. Cloupeau, B. Prunet-Foch, *J. Aerosol Sci.* **25**, 1021 (1994).
19. J. B. Fenn, M. Mann, C. K. Meng, S. F. Wong, *Science* **246**, 64 (1989).
20. A. M. Gañán-Calvo, J. Dávila, A. Barrero, *J. Aerosol Sci.* **28**, 249 (1997).
21. I. G. Loscertales, J. Fernández de la Mora, in *Synthesis and Measurement of Ultrafine Particles*, J. Marijnissen, S. Pratsinis, Eds. (Delft Univ. Press, Delft, Netherlands, 1993), pp. 115–118.
22. J. R. Lister, *J. Fluid Mech.* **198**, 231 (1989).
23. S. Blake, G. N. Ivey, *J. Volcanol. Geotherm. Res.* **27**, 153 (1986).
24. I. Cohen, H. Li, J. L. Hougland, M. Mrksich, S. R. Nagel, *Science* **292**, 265 (2001).
25. A. M. Gañán-Calvo, *Phys. Rev. Lett.* **80**, 285 (1997).
26. ———, A. Barrero, *J. Aerosol Sci.* **30**, 117 (1999).
27. I. G. Loscertales, R. Cortijo, A. Barrero, A. M. Gañán-Calvo, Spanish Patent Application P2001-00231 (2001).
28. The range of values of the applied electrical potential and injected flow rates required to obtain a structured Taylor cone depends on the physical properties of the liquids (mainly electrical conductivities, viscosities, and surface tensions; 6.2×10^{-5} S m^{-1} and 0.6 kg $m^{-1} s^{-1}$ are the electrical conductivity and viscosity of Somos, and 43 mN m^{-1} is the Somos-air interfacial tension) and the geometry of the system (mainly the needle-to-collector distance). In our experiments, the diameters of the needles were 1 mm outer diameter (OD) and 0.7 mm inner diameter (ID) (outer needle) and 0.4 mm OD and 0.25 mm ID (inner needle). Silica tubing (0.35 mm OD, 0.075 mm ID) was also used as the inner needle in the experiments with water-oil. The needle-to-collector distance ranged between about 0.8 and 1.4 mm. Typical values of the voltages used in the experiments shown in Figs. 2 to 6 range between 3 and 5 kV. Typical values of the liquid flow rates are given in Figs. 3 and 6.
29. The use of liquids with much less viscosity may lead to intense flow recirculations inside the Taylor cone (*36*).
30. The only way liquid insulators can be electrosprayed in the cone-jet mode is by artificially increasing their electrical conductivity via additives.
31. J. Fernández de la Mora, I. G. Loscertales, *J. Fluid Mech.* **260**, 155 (1994).
32. J. Rosell-Llompart, J. Fernández de la Mora, *J. Aerosol Sci.* **25**, 1093 (1994).
33. J. Rosell-Lompart, I. G. Loscertales, D. Bingham, J. Fernández de la Mora, *J. Aerosol Sci.* **27**, 695 (1996).
34. I. G. Loscertales, J. Fernández de la Mora, *J. Chem. Phys.* **103**, 5041 (1995).
35. M. Gamero-Castaño, J. Fernández de la Mora, *Anal. Chim. Acta* **406**, 67 (2000).
36. A. Barrero, A. M. Gañán-Calvo, J. Dávila, A. Palacio, E. Gómez-González, *Phys. Rev. E* **58**, 7309 (1998).

37. Two of the authors (I.G.L.) and (A.B.) thank J. Fernández de la Mora, J. M. López-Herrera, A. Garrido, and M. González for their valuable assistance. One of the authors (M.M.) dedicates this work to G. Chuchani on his 77th anniversary.

31 October 2001; accepted 24 January 2002

A Thermally Re-mendable Cross-Linked Polymeric Material

Xiangxu Chen,[1] Matheus A. Dam,[1] Kanji Ono,[2] Ajit Mal,[3] Hongbin Shen,[4] Steven R. Nutt,[4] Kevin Sheran,[1] Fred Wudl[1]*

We have developed a transparent organic polymeric material that can repeatedly mend or "re-mend" itself under mild conditions. The material is a tough solid at room temperature and below with mechanical properties equaling those of commercial epoxy resins. At temperatures above 120°C, approximately 30% (as determined by solid-state nuclear magnetic resonance spectroscopy) of "intermonomer" linkages disconnect but then reconnect upon cooling. This process is fully reversible and can be used to restore a fractured part of the polymer multiple times, and it does not require additional ingredients such as a catalyst, additional monomer, or special surface treatment of the fractured interface.

In past decades, highly cross-linked polymers have been studied widely as matrices for composites, foamed structures, structural adhesives, insulators for electronic packaging, etc. (*1*, *2*). The densely cross-linked structures are the basis of superior mechanical properties such as high modulus, high fracture strength, and solvent resistance. However, these materials are irreversibly damaged by high stresses (*3*, *4*) due to the formation and propagation of cracks. The latter lead to dangerous loss in the load-carrying capacity of poly-

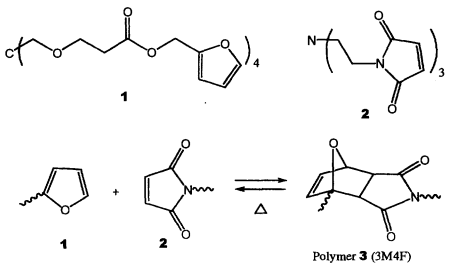

Scheme 1.

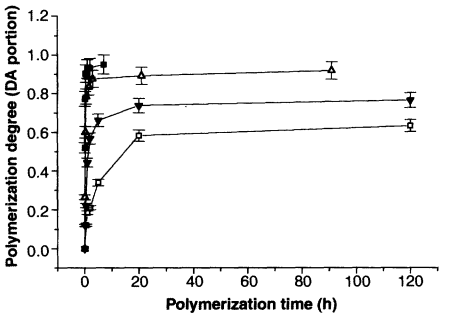

Fig. 1. Polymerization degree versus time. (□) 24°C; (▼) 45°C; (△) 60°C; (■) 75°C.

meric structural engineering materials (*5*, *6*).

The exploration of re-mending and self-healing of polymeric materials has become increasingly more exciting in the recent past, culminating in a genuinely self-healing material (*4*). The hot plate welding and crack healing of thermoplastics, where intermolecular noncovalent interactions (chain entanglements) at the interface are responsible for mending, have been well established (*7*–*9*). Small molecules–induced crack healing has also been studied for thermoplastics (*10*, *11*), and a composite of a linear polymer with a thermoset that has crack-healing ability was reported (*12*). The concept of self-repair was introduced to heal cracks by embedding hollow fibers that can release repair chemicals when a crack propagates (*7*, *13*, *14*). The most recent report of crack self-healing (autonomic healing) of an epoxy resin consists of a clever use of catalytic network formation of an encapsulated add-monomer, which is held within a capsule embedded in the epoxy matrix (*4*). But questions remain concerning the long-term stability of the catalyst and the ability of the material to self-heal multiple times. We describe a truly "re-mending" material consisting of a highly cross-linked, transparent polymer that exhibits multiple cycles of autonomic crack mending with simple, uncatalyzed thermal treatment and forms covalent bonds at the interface of the mended parts. In contrast, in hot plate welding and crack healing of thermoplastics, only intermolecular, noncovalent interactions (chain entanglements, hydrogen bonding, etc.) are responsible for the mend and no new covalent bonds are formed between the mended parts.

Thermally reversible reactions, particularly the Diels-Alder (DA) reaction, for cross-linking linear polymers have been pioneered and studied by Kennedy and Wagener during the past two decades (*15*–*21*). To the best of our knowledge, as shown in all the reports of thermoreversible polymers, cross-linkable and reversible groups were attached to linear polymer backbones, but the connections of the cross-linkers to the polymer backbones were not reversible (*15*–*21*). In contrast, we report a macromolecular network formed in its entirety by reversible cross-linking covalent bonds.

A thermally reversible DA cycloaddition of a multi-diene (multi-furan, F) and multi-dienophile (multi-maleimide, M) was used to prepare a polymeric material (Scheme 1). Monomer **1** (4F) contains four furan moieties on each molecule, and monomer **2** (3M) includes three maleimide moieties on each molecule (*22*). A highly cross-linked network (polymer **3**, 3M4F) can be formed via the DA reaction of furan and maleimide moieties, and thermal reversibility can be accomplished by the retro-DA reaction (*23*).

A dichloromethane solution of monomers **1** and **2** (with stoichiometric F:M ratio) was poured into a glass mold or cast on a quartz plate. Vacuum evaporation of the solvent at room temperature followed by heating produced the macromolecular solid. Polymerization at different temperatures was studied by ultraviolet (UV) spectroscopy. Monoliths of polymeric material were obtained by breaking the glass mold, whereas thin films were produced when cast on quartz substrates. Because the polymerization process involves the formation of DA adducts, the efficiency of the DA reaction can be used to study the degree of polymerization. According to the literature (*19*), the extent of the DA reaction for a similar system could be followed quantitatively by UV spectroscopy, and the degree of cross-linking as a function of reaction temperature is shown in Fig. 1. At 24°C, polymerization of up to 60 to 70% required 5 days. The polymerization–cross-linking process is much faster at higher temperatures, reaching "completion" (95% ± 5%) in just 3 hours at 75°C.

Differential scanning calorimetry (DSC) showed that the polymerization process is exothermic by 23 kcal/mol (per DA adduct) (*24*). Assuming the principle of microscopic reversibility applies, this result implies that upon heating the retro-DA reaction is an accessible reaction pathway that is preferred over (nonreversible) bond-breaking degradation reactions (*25*) in the polymer network.

The bulk polymeric material is hard and fully transparent, with a density of 1.37 g/cm^3 and an index of refraction of 1.56 at 24°C. On the basis of a nondestructive ultrasonics technique (*26*), the Young's modulus and Poisson ratio were determined to be 4.72 GPa and 0.349, respectively. From the results shown in Table 1, it is clear that the mechanical properties of this polymer are in the range of commercial, state-of-the-art, cross-linked epoxy resins and unsaturated polyesters (*1*, *32*).

Solid state reversibility (*27*), was tested via a series of heating cycles that consisted of heating fully polymerized films to different temperatures on quartz substrates and then quenching in liquid nitrogen. After the heat-quench procedure, the samples were heated at 80°C, causing repolymerization and/or cross-linking of the films. The results of five such cycles are shown in Fig. 2. About 25% of the DA adducts disconnected after thermal treatment at 150°C, but only ~12% did so after treatment at 130°C (first half cycle, left side of Fig. 2). Under these conditions, the sample was observed to be irreversible below 120°C. Prolonged storage of the films at 80°C afford-

Table 1. Mechanical properties of polymer **3** compared with epoxy resins [data taken from p. 250 of (*1*)] and unsaturated polyesters (Unsat. poly.) [data taken from p. 250 of (*1*)]. Methods follow the guidelines of the American Society for Testing and Materials (ASTM). Dashes indicate data not reliable by method used.

Properties	Polymer **3**	Epoxy resins	Unsat. poly.	Methods
Tensile				D638
Strength (MPa)	68*	27 to 88	4 to 88	Type V
Modulus (GPa)	—	2.4	2 to 4.4	
Elongation (%)	1.6 to 4.7	3 to 6	<2.6	
Compression				D695
Strength (MPa)	121*	102 to 170	88 to 204	
Modulus (GPa)	3.1	3.4†		
Flexural				D790
Strength (MPa)	143*	88 to 143	58 to 156	
Modulus (GPa)	—		3.4 to 4.2‡	

*Strength at yield. †Cycloaliphatic casting; value taken from p. 91 (*32*). ‡Rigid; data taken from p. 464 (*32*).

[1]Exotic Materials Institute and Department of Chemistry and Biochemistry, [2]Department of Materials Science and Engineering, [3]Department of Mechanical and Aerospace Engineering, University of California, Los Angeles, 405 Hilgard Avenue, Los Angeles, CA 90095, USA. [4]Department of Materials Science, University of Southern California, Los Angeles, CA 90089, USA.

*To whom correspondence should be addressed. E-mail: wudl@chem.ucla.edu

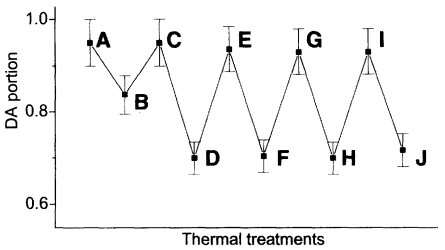

Fig. 2. Thermal reversibility of polymer **3**. (**A**) to (**B**), 130°C for 25 min, followed by quenching in liquid nitrogen. (B) to (**C**), (**D**) to (**E**), (F) to (**G**), and (**H**) to (**I**), 80°C for 1 hour. (C) to (D), (E) to (F), (G) to (H), and (I) to (**J**), 150°C for 15 min, followed by quenching in liquid nitrogen.

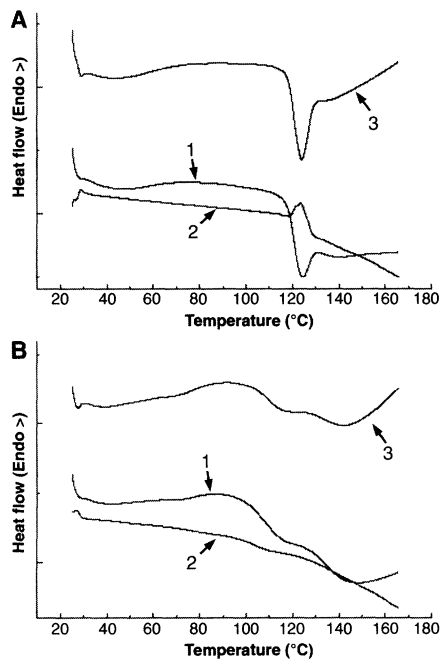

Fig. 3. Modulated DSC data of polymer **3** (scanning rate, 5°C/min). (**A**) Sample was cooled from 145° to 24°C in 24 hours. (**B**) Sample was heated to 145°C for 25 min and then quenched in liquid nitrogen. "1" marks total heat flow; "2," reversing heat flow; "3," nonreversing heat flow.

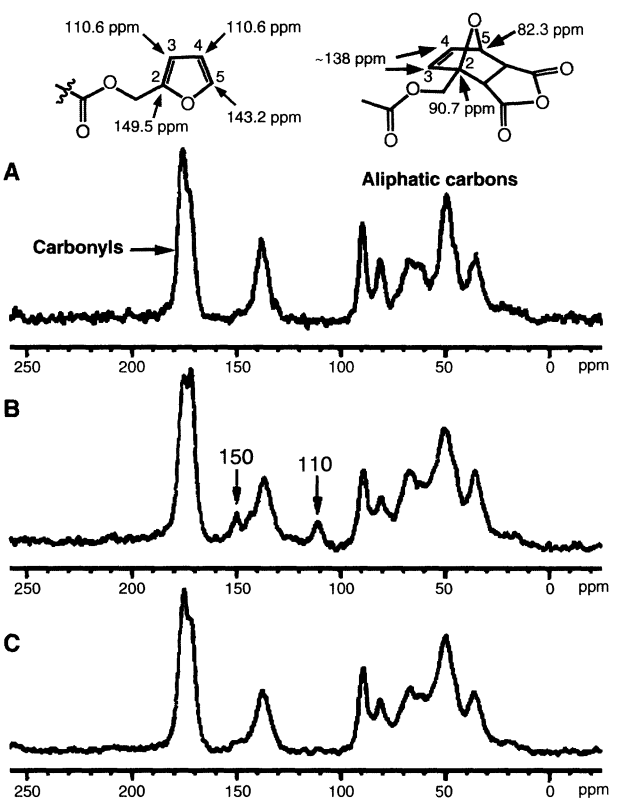

Fig. 4. Solid State ^{13}C-NMR spectra of (**A**) a fully polymerized sample, (**B**) a sample heated to 145°C and then quenched in liquid nitrogen, and (**C**) a repolymerized sample (cooled from 120° to 70°C in 24 hours).

ed full reconnection of the DA partners. Clearly, the simplest interpretation of these five continuous cycles demands that the DA and retro-DA reactions are reversible in this extended solid.

As shown in Fig. 3, samples with different thermal history were studied by temperature-modulated DSC (TMDSC). This type of thermal analysis is used to determine and distinguish between (i) fully reversible heat effects that are related to the heat capacity change and (ii) time-dependent irreversible heat effects that are related to kinetics (*28*, *29*). In Fig. 3A, a fully polymerized sample, which was cooled from 145° to 25°C in 24 hours, showed only an endothermic peak at 124°C. The shape is typical for physical aging effects (*30*). A sample that was kept at 145°C for 25 min and quenched in liquid nitrogen showed an exothermic peak from 60° to 120°C on the nonreversing heat flow curve (Fig. 3B). These results indicate that the quenched sample contains disconnected furan and maleimide moieties, and, as the molecular chains gain enough mobility at increased temperature, they reconnect efficiently. At temperatures above 120°C, endothermic peaks in both nonreversing heat flows (due to the retro-DA reaction in the network) were observed.

Solid state ^{13}C-NMR spectroscopy was also used to study the thermally reversible DA reaction of the macromolecular solid. Solution ^{13}C-NMR spectroscopy of the 4F monomer revealed resonances for positions 2, 3, 4, and 5 of the furan moieties at 149.5, 110.6, 110.6, and 143.2 parts per million (ppm), respectively. Upon cycloaddition, the C-3 and C-4 positions shift to around 138 ppm, and the C-2 and C-5 resonances shift up-field (82.4 and 90.7 ppm). To confirm our assignments, the DA adduct of furfuryl acetate with maleic anhydride was used as a model system (see structures with Fig. 4). Solid state ^{13}C-NMR spectra of polymer **3** as a function of thermal cycling are shown in Fig. 4. Figure 4A is a spectrum of the fully polymerized extended solid with a clear absence of peaks at 110 and 150 ppm. Heating the polymer to 145°C for 25 min and then quenching in liquid nitrogen produced material with the solid state ^{13}C-NMR spectrum shown in Fig. 4B. The ~ 110 and ~150 ppm resonances are visible, indicating the presence of unreacted furan moieties. The same sample was heated to 120°C and cooled down to 70°C in 24 hours to repolymerize. Its solid state ^{13}C-NMR spectrum is shown in Fig. 4C. Because the latter is essentially identical to the spectrum in Fig. 4A and no peaks due to furan moieties were observed, the simplest interpretation demands that, within the experimental error of solid state NMR spectroscopy, all the disconnected linkages had reconnected.

Because the bond strength between diene and dienophile of the DA adduct is much lower than all the other covalent bonds, the retro-DA reaction should be the major reason for crack propagation. In principle, when the sample is reheated, the furan and maleimide moieties should reconnect and the cracks, or fractures, should mend.

To determine the fracture-mending efficiency of this polymer, tests were performed with the use of compact tension test specimens (*4*, *12*, *31*) (Fig. 5). A sharp pre-crack was created in the tapered samples by gently tapping a fresh razor blade into a machined starter notch. Application of a load in the direction perpendicular to the pre-crack, led to a fracture of the specimen because it was not possible to stop the crack propagation. After structural failure, the two pieces were matched as closely as possible and were held together with a clamp, treated at 120° to 150°C under nitrogen for about 2 hours, and cooled to room temperature. Photographs of the

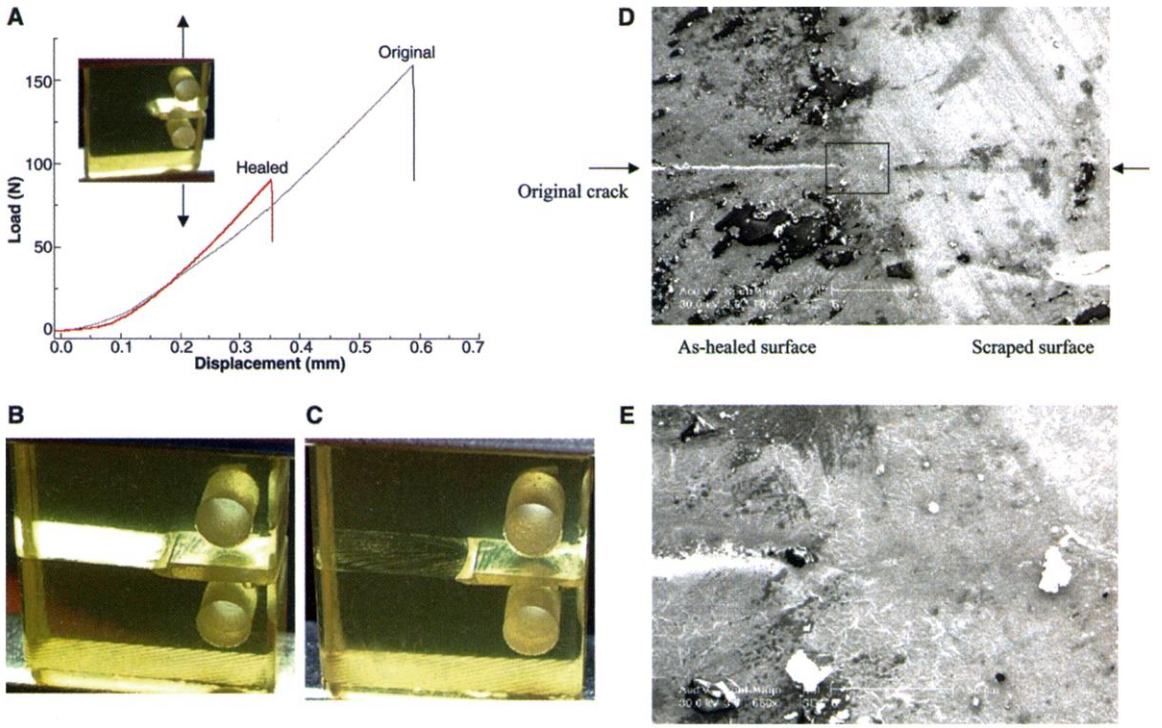

Fig. 5. Mending efficiency of polymer **3**. (**A**) Mending efficiency obtained by fracture toughness testing of compact tension test specimens. Values for the original and healed fracture toughness were determined by the propagation of the starter crack along the middle plane of the specimen at the critical load. (**B**) Image of a broken specimen before thermal treatment. (**C**) Image of the specimen after thermal treatment. (**D**) SEM image of the surface of a healed sample: the left side is the as-healed surface and the right side is the scraped surface. (**E**) Enlarged image of the boxed area in (D).

mending effect of a typical specimen are shown in Fig. 5, B and C. Before mending, the interface of the crack was highly reflectant (Fig. 5B). After thermal treatment, only a slight interface mismatch was observable (Fig. 5C), indicating mending (healing) of the interface.

Scanning electron microscope (SEM) images of a healed sample are also shown in Fig. 5, D and E. Before the images were taken, Cr (3 nm) and Au (30 nm) were deposited onto the surface via electron-beam evaporation. Shown on the left side of Fig. 5D is the scar of the mended interface; the right side is where the surface was scraped with a fresh razor blade. Because the two pieces that were mended could not be matched perfectly when held together, the scar on the healed surface is clearly visible as a white line. However, the surface scraped with the razor blade reveals that the fracture healed almost completely to produce a homogeneous material with a few minor defects, suggesting remarkable mending efficiency. Figure 5E is an enlarged image of Fig. 5D. The latter shows the interface between the scarred section and the scraped section, and it gives a clearer, more dramatic view of the mending effect.

Fracture tests were also carried out in an effort to quantify the healing efficiency (*4*). Representative load-displacement curves for a polymer specimen are plotted in Fig. 5A, showing recovery of about 57% of the original fracture load. Not surprisingly, the accurate replacing of the two halves and thermal treatment temperatures affected the mending efficiencies. At 150°C, an average mending efficiency of about 50% was achieved, whereas at 120°C the average value was 41%. Considering that the specimens were split into two separate pieces and kept under the same atmospheric pressure sometimes as long as 24 hours, the mending efficiencies are impressive when compared with crack healing of thermoplastic elastomers (*12*), but they are not as high as those reported for White's composite (*4*). Another factor, which should affect healing efficiency, is the uniformity and amount of applied pressure. Our preliminary results indicate that the effect of pressure appears to be minimal. The fracture and mending processes of each independently prepared specimen were carried out at least two times. Within experimental error, the critical load at fracture of the third cracking was about 80% of the second, strongly suggesting that this material can be healed efficiently multiple times. The second and third crack usually propagated along the original crack plane. However, it was not uncommon to observe cracking in a region adjacent to a scar from a previous crack. This is probably due to the fact that the healed region has different mechanical properties than the original material and is a result of the unique covalent interfacial bonding.

To test oxidative degradation of the polymer we performed some accelerated tests by heating specimens in air (at standard pressure) to 120° or 130°C and then performing compression testing. Within the experimental error of the test, the mechanical properties showed only minor changes. Though polymeric material **3** has the desirable and unusual properties described above, it has shortcomings as follows that are being improved for next generations: (i) the maleimide monomer melts at too high a temperature, is colored (yellow), and is insoluble in monomer 4F. (ii) Though polymer **3** can be cured in less than an hour at 130°C, a full curing of it takes hours to complete. (iii) The service temperature of polymer **3** is 80° to 120°C, which may be too low for many applications but close to ideal for others, such as self-mending electronic packaging, where cracking occurs due to differences in thermal index of expansion.

References and Notes

1. S. H. Goodman, Ed., *Handbook of Thermoset Plastics* (Noyes, Park Ridge, NJ, ed. 2, 1998).
2. T. Kaiser, *Prog. Polym. Sci.* **14**, 373 (1989).
3. J. A. Sauer, M. Hara, *Adv. Polym. Sci.* **91/92**, 69 (1990).
4. S. R. White *et al.*, *Nature* **409**, 794 (2001).
5. R. Talreja, Ed., *Damage Mechanics of Composite Materials* (Elsevier, Amsterdam, 1994), pp. 139–241.
6. A. J. Kinloch, *Adv. Polym. Sci.* **72**, 45 (1985).
7. R. P. Wool, *Polymer Interfaces: Structure and Strength* (Hanser Gardner, Cincinnati, 1995), pp. 445–479.
8. C. B. Bucknall, I. C. Drinkwater, G. R. Smith, *Polym. Eng. Sci.* **20**, 432 (1980).
9. K. Jud, H. H. Kausch, J. G. Williams, *J. Mater. Sci.* **16**, 204 (1981).
10. E. P. Wang, S. Lee, J. Harmon, *J. Polym. Sci. Polym. Phys. Ed. B* **32**, 1217 (1994).
11. C. B. Lin, S. Lee, K. S. Liu, *Polym. Eng. Sci.* **30**, 1399 (1990).
12. J. Raghavan, R. P. Wool, *J. Appl. Polym. Sci.* **71**, 775 (1999). A composite with dual phase structure of linear polystyrene and cross-linked vinyl ester was studied. Of the critical strain energy, 1.7% was recovered after annealing of fracture solid interfaces, which we believe is from polystyrene chain interpenetration.
13. C. M. Dry, N. Sottos, *Smart Structures and Materials 1993: Smart Materials*, SPIE Proceedings 1916, 1 to 4 February 1993, Albuquerque, NM, V. K. Varadan, Ed. (SPIE, Bellingham, WA, 1993), p. 438.

14. C. Dry, *Comp. Struct.* **35**, 263 (1996).
15. L. P. Engle, K. B. Wagener, *J. Macromol. Sci. Rev. Macromol. Chem.* **C33 (3)**, 239 (1993).
16. J. P. Kennedy, K. F. Castner, *J. Polym. Sci., Polym. Chem. Ed.* **17**, 2039 (1979).
17. Y. Chujo, K. Sada, T. Saegusa, *Macromolecules* **23**, 2636 (1990).
18. J. R. Jones, C. L. Liotta, D. M. Collard, D. A. Schiraldi, *Macromolecules* **32**, 5786 (1999).
19. Y. Imai, H. Itoh, K. Naka, Y. Chujo, *Macromolecules* **33**, 4343 (2000).
20. J. R. McElhanon, D. R. Wheeler, *Org. Lett.* **3**, 2681 (2001)
21. C. Goussé, A. Gandini, P. Hodge, *Macromolecules* **31**, 314 (1998).
22. The synthesis procedures for compounds **1** (liquid at 24°C) and **2** (mp, 113° to 114°C) and for polymer **3** are available in the supplemental material, available on *Science* Online at www.sciencemag.org/cgi/content/full/295/5560/1698/DC1.
23. B. Rickborn, *Org. React.* **52**, 1 (1998).
24. J. M. Barton, *Adv. Polym. Sci.* **72**, 111 (1985).
25. N. S. Isaacs, *Physical Organic Chemistry* (Longman Scientific and Technical, 1997).
26. R. C. McMaster, Ed., *Nondestructive Testing Handbook* (American Society for Nondestructive Testing, ed. 2, 1982). The ultrasonics method takes advantage of the direct relation between mechanical properties (Young's modulus) and the propagation velocity of ultrasound through the material.
27. Whereas in the solid state the reversibility is observable only to the extent of ~ 10% to 20% (see Fig. 4, A and B), a suspension of a 350 mg sample of a monolith in 50 ml chlorobenzene dissolved completely upon heating to reflux over ~1 hour.
28. M. Ribeiro, J.-P. E. Grolier, *J. Therm. Anal. Cal.* **57**, 253 (1999).
29. M. Pyda, B. Wunderlich, *J. Polym. Sci. Polym. Phys. Ed. B* **38**, 622 (2000).
30. M. Song, *J. Therm. Anal. Cal.* **63**, 699 (2001).
31. The compact tension test specimens were made according to the literature [Y. Murakami, Ed., *Stress Intensity Factors Handbook* (Pergamon, Tokyo, 1987), vol. 1, p. 18], with W = 12 mm, t = 6 mm and $a/W \approx 0.4$, where W is width, t is thickness, and a is length of notch. The fracture toughness (K_{Ic}) can be determined as $K_{Ic} = \alpha P_c$ where α is a geometry and materials property, which can be calculated from the equation shown in the work cited in this reference, and P_c is the critical load at fracture (*4*). α was measured to be 1.1×10^4 $m^{-3/2}$. The fracture energy (G_{Ic}) value can be calculated according to the literature (*7*), $G_{Ic} = (1 - \nu^2) K_{Ic}^2/E$, where ν is the Poisson ratio and E is Young's modulus. Therefore, in terms of fracture energy, the best value of re-mending efficiency was 32%, and the average efficiency for a number of specimens (after thermal treatment at 150°C) was 25%.
32. J. E. Mark, Ed., *Polymer Data Handbook* (Oxford Univ. Press, New York, 1999), pp. 91 and 464.
33. We thank NSF for support through a grant (DMR 976302). We also thank J. R. Heath and R. Beckman for SEM images, W. P. Weber for thermal mechanical analysis, and C. E. Hoyle and C. Nguyen for constructive discussions on the synthesis of compounds with maleimide moieties.

30 August 2001; accepted 30 January 2002

Protein Nanoarrays Generated By Dip-Pen Nanolithography

Ki-Bum Lee,[1] So-Jung Park,[1] Chad A. Mirkin,[1]* Jennifer C. Smith,[2] Milan Mrksich[2]*

Dip-pen nanolithography was used to construct arrays of proteins with 100- to 350-nanometer features. These nanoarrays exhibit almost no detectable nonspecific binding of proteins to their passivated portions even in complex mixtures of proteins, and therefore provide the opportunity to study a variety of surface-mediated biological recognition processes. For example, reactions involving the protein features and antigens in complex solutions can be screened easily by atomic force microscopy. As further proof-of-concept, these arrays were used to study cellular adhesion at the submicrometer scale.

Arrays of microscopic features comprising different proteins are extremely important for proteomics and cell research, pharmaceutical screening processes (*1–4*), and panel immunoassays (*5, 6*). Many conventional patterning techniques, including photolithography (*6, 7*), microcontact printing (*2, 8*), and spot arraying (*1*), have been used for fabricating such arrays. Submicrometer spot arrays of proteins have been generated by finely focused ion beam lithography (FFIB) (*9*), and individual micrometer and submicrometer features have been prepared by atomic force microscopy (AFM) techniques with varying degrees of success (*10–14*). One of the advantages of miniaturization is that when a feature composed of receptors is miniaturized to the scale of the biological analytes, new methods for screening reactions involving such receptors and analytes become available, because almost every physical property of the receptor feature is changed upon reaction with the analyte, including the height, hydrophobicity, roughness, and shape of each feature, which are all variables easily probed with a conventional AFM. One disadvantage of receptor feature miniaturization in such an array is that nonspecific binding of the protein array can become a major problem leading to large background signals. For example, it could be difficult to differentiate inactive areas of the substrate that experience such binding from the active receptor features, thereby complicating the analysis of the nanoscale libraries. Indeed, others who have attempted to study reactions involving antibodies and antigens on a surface with an AFM have noted the importance of eliminating nonspecific binding when studying individual nano- and micrometer-scale protein features (*10–13*). Here, we describe how a high-resolution patterning technique, dip-pen nanolithography (DPN), can be used to construct nanoarrays of proteins. Moreover, we demonstrate that these arrays can be fabricated with almost no detectable nonspecific binding of proteins to the passivated portions of the array, even in solutions containing multiple proteins, and that reactions involving the protein features and antigens can be screened by AFM. Finally, we show how such nanoarrays can be implemented in the study of cellular interactions with nanopatterned surfaces.

A typical protein array was fabricated by initially patterning 16-mercaptohexadecanoic acid (MHA) on a gold thin-film substrate in the form of dots or grids. The features studied thus far, both lines and dots, have been as large as 350 nm (line width and dot diameter, respectively) and as small as 100 nm (Fig. 1). The areas surrounding these features were passivated with 11-mercaptoundecyl-tri(ethylene glycol) by placing a droplet of a 10 mM ethanolic solution of the surfactant on the patterned area for 45 min followed by copious rinsing with ethanol and, then, NANOpure water (NANOpure, Barnstead/Thermolyne Corp.). As proof-of-concept experiments, the proteins were absorbed on the preformed MHA patterns (Fig. 2) by immersing the substrate in a solution containing the desired protein (10 μg/ml) for 1 hour. The substrate was then removed and rinsed with 10 mM Tris buffer [Tris-(hydroxymethly) aminomethane], Tween-20 solution (0.05%) and, finally, NANOpure water. Such proteins have a high affinity for carboxylic acid–terminated monolayers at pH 7 (*10–13*) and a relatively weak affinity for surfaces coated with 11-mercaptoundecyl-tri(ethylene glycol) (*15, 16*). The protein arrays were then characterized by AFM. In the case of arrays composed of immunoglobulin G (IgG) patterns, the reaction of the array with rabbit antibody to mixtures of proteins was studied by AFM.

Lysozyme, an ellipsoidal shaped protein (4.5 nm by 3.0 nm by 3.0 nm), (*17*) cleanly assembled on the MHA nanopatterns, as evidenced by contact and tapping mode AFM (Fig. 1, B to D), respectively (*18*). Note that there is almost no evidence of nonspecific

[1]Northwestern University, Department of Chemistry and Center for Nanofabrication and Molecular Self-Assembly, 2145 Sheridan Road, Evanston, IL 60208, USA. [2]University of Chicago, Department of Chemistry and the Institute for Biophysical Dynamics, 5735 South Ellis, Chicago, IL 60637, USA.

*To whom correspondence should be addressed. E-mail: camirkin@chem.northwestern.edu; for cell adhesion work: mmrksich@midway.uchicago.edu